Effect of Si-Ni-P on the emergence of dislocations loops in Fe-9Cr matrix under neutron irradiation: TEM study and OKMC modelling

A. Dubinko[1], N. Castin[1], D. Terentyev[1], G. Bonny[1], M. J. Konstantinović[1]

[1] SCK•CEN, Nuclear Materials Science Institute, Boeretang 200, B-2400 Mol, Belgium

Abstract

The expected degradation of mechanical properties of structural materials under irradiation (i.e. "in operation") in nuclear components represents a significant challenge for the design to account the impact of long-term irradiation effects. Therefore, a development of scientific and engineering expertise to understand and possibly control the severe impact of harsh neutron irradiation on materials is one of the tasks in the current material's research agenda. As it is well known from long-standing experience with fission systems, radiation embrittlement is caused by nano-scale features that obstruct plasticity mediated by dislocations. The present contribution highlights recent research and development efforts addressed towards the assessment of the interrelation between nano-structural features and hardening induced by neutron irradiation in fusion structural high-Cr ferritic/martensitic steels.

In this work, the impact of doping by three chemical elements (nickel, silicon and phosphorus) on the microstructural evolution under neutron irradiation at 300°C and 450°C is studied experimentally as well as by computer simulations. The evolution of microstructure is assessed by transmission electron microscopy and object kinetic Monte Carlo simulations. The latter method utilizes a new approach enabling to follow both nano-scale irradiation defects and micro-segregation zones causing the formation of solute rich clusters, detectable by atom probe tomography. The results of the present work clearly point out that Ni-Si segregation alters the spatial and size distribution of dislocations loops already at as low dose as 0.1 dpa. The physical mechanisms behind the impact of minor alloying elements are discussed.

Keywords: ferritic steel; precipitation; irradiation; TEM; modelling

*Author for correspondence. Email: adubinko@sckcen.be, Tel.: +32-14-333185

1. Introduction

Radiation-induced embrittlement in materials with structural functions such as ferritic/bainitic/martensitic/austenitic steels, nickel-based alloys, zirconium-based alloys and aluminum pipes is often the lifetime limiting factor of their operation [1]. Under neutron irradiation, the primary mechanism of embrittlement is the obstruction of dislocation motion by nano-metric defect structures which develop as a result of atomic mixing and solute/defect diffusion taking place continuously under irradiation [2, 3]. Any commercial structural material contains a number of solute elements which are added intentionally (to improve certain

properties) or are residual impurities (unavoidable in commercial production). Given that different chemical elements exhibit different affinity to radiation defects, there is a mutual relationship between the evolution of irradiation defects and nano-scale chemical rearrangement (i.e. segregation zones, precipitation) under irradiation. The eventual microstructure will be determined by the irradiation flux, fluence, chemical composition and initial microstructure of the material (i.e. dislocation density and grain size) [2]. In the case of the most common nuclear structural materials – iron-based steels (like reactor pressure vessel and high-chromium ferritic martensitic steels), it is by now accepted that two classes of nano-structural features contribute to its embrittlement: (i) solute rich clusters (SRC) and (ii) the so-called *matrix damage*, interpreted as the clustering of point-defects eventually yielding to dislocation loops and voids [4-7].

Over the recent years, a lot of attention was drawn to the SRC type defects. The SRC features are hardly resolvable by transmission electron microscopy, but well detected by atom probe tomography techniques applied to both currently operating reactor pressure vessel steels and future generation ferritic martensitic/austenitic steels [8-16]. The above noted works underline that SRCs are present in high density so that their contribution to the resulting hardening (and as consequence embrittlement) can be dominating at low doses and represent significant fraction (up to 50%) at intermediate irradiation doses (~1 dpa). In particular, it has been discussed that in the case of ferritic martensitic 9Cr matrix, silicon, nickel and phosphorus (Si-Ni-P) exhibit irradiation induced segregation causing extra hardening in the irradiation dose range 0.1-1 dpa [9, 11, 17, 18]. This is why a proper understanding of the role played by these chemical elements on the onset of irradiation microstructure development is an important part of the complete assessment and reliable prediction of the irradiation-induced microstructural evolution at the component lifetime scale.

With this aim in mind, the mechanical properties of neutron irradiated fully ferritic Fe-Cr ferritic model alloys, together with actual 9%Cr F/M alloys and steels, with varying concentrations of Cr, Ni, Si and P, have been recently investigated [40]. The focus was on the effect on radiation hardening of the content of Cr and minor solutes such as Ni, Si and P as well as on initial microstrucutre. Irrespective of irradiation temperature and of the Cr content, significant hardening was observed only in model alloys containing Ni, Si and P solute atoms. This observation strongly suggests that Cr solutes play lesser role in irradiation hardening of F/M alloys steels than previously believed. The presence of minor solutes (Ni, Si, P) was found to be essential for the microstructural features that form under irradiation to have a hardening effect, i.e. to make the features efficient obstacles to dislocation motion. Additionally, it was observed that the martensitic alloys harden much less than the ferritic ones [40].

One of the hypotheses behind the formation of the SRC defects is the segregation of solutes transferred by point defects to nano-metric dislocation loops (DLs) and self-interstitial atom clusters [19-22]. Dedicated atomistic molecular dynamics (MD) studies have proved that solute segregation indeed increases the strength of the irradiation defects as obstacles for a moving dislocations [18, 23-26]. This explains the importance of introduction of the mechanisms in microstructural simulation tools enabling to study the radiation induced segregation simultaneously with the accumulation of loop/voids, which is conventional output.

Kinetic Monte Carlo models (KMC) [27-31] allow to integrate the reactions undertaken by irradiation-induced defects and other phenomena that take place under irradiation caused by atomic rearrangement (e.g. solute transport, segregation, precipitation, etc.). In particular, the Object KMC (OKMC) method [29-31] encompasses all the necessary time and length scales to fully describe the effects of neutron irradiation, from the primary damage (atomic collision cascades resulting from bombarding particles) to the formation of solute clusters resulting from

long-range diffusion and transport processes [32]. Clearly, such models are crucial for rationalizing the experimental evidences, revealing the dominating mechanisms taking place in metals under irradiation.

In this work, we perform a combined study employing neutron irradiation experiment, transmission electron microscopy (TEM) and object kinetic Monte Carlo (OKMC) simulations to investigate the impact of the variation of Si-Ni-P content in the Fe-9Cr matrix under neutron irradiation. The irradiation conditions are chosen in line with target operation temperature for such materials being in the range of 300°C-450°C, where 300°C is typical lower bound operation for water cooled components [33] and 350-450°C is the operational temperature in the liquid metal environment [34], which is essential for fission GEN IV reactors. To catch the onset of the irradiation damage, we have opted to perform irradiation up to 0.1 dpa, which is known to be significant enough to cause the observation of the primary irradiation damage at least at 300°C in this class of materials [35, 36], yet low enough not to observe intensive development of dislocation loop rafts and void swelling. The low level of damage also enables us to proceed with experiments straight after the irradiation without losing the time for cooling down. TEM results are rationalized using a new object kinetic Monte Carlo (OKMC) method [37] which couples the atomic and defect fluxes thus offering the description of irradiation induced diffusion and segregation at irradiation defects. The OKMC tool is applied to explore the role played by Ni-Si-P impurities, accounting for realistic material microstructure, particular irradiation conditions and available TEM information.

2. Methods and Materials.

2.1 Materials and irradiation conditions.

Two model alloys with different Ni-Si-P contents whose composition is shown in Table 1 were fabricated by OCAS NV (Belgium). Neutron irradiation was performed in the Belgian nuclear reactor 2 (BR2) of SCK CEN in Mol. Details on material fabrication and neutron irradiation were published in Ref. [40]. In addition to those alloys, we used electrolytic pure iron which was investigated in our earlier works [38, 39]. The details of the chemical composition and fabrication route could be found in these Ref [11, 35].

Table 1. Composition of the studied materials.

ID	***Short name***	***Cr*** *w%*	***Ni*** *w%*	***Si*** *w%*	***P*** *w%*	***Al*** *w%*
G379	Fe*	0.002	0.007	0.001	0.003	0.023
G385	Fe-9Cr	9.1	0.009	0.004	0.003	0.027
G389	Fe-9Cr-NiSiP	9.1	0.092	0.212	0.032	0.028

* G379 is electrolytic pure Fe with wt% content of residual impurities not exceeding: 0.005C, 0.005N, 0.005Si, 0.005P, 0.005Ni, 0.00S.

The neutron flux was around 1.5 x 10^{13} n/cm^2/s, reaching a fluence level of about 1.1 x 10^{20} n/cm^2 during two consequtive 3-week reactor cycles. The neutron irradiation has been performed at two temperatures, 290 and 450 ^{0}C. The temperature of 290 ^{0}C was guaranteed by the temperature of the flowing water through the CALLISTO loop, while the temperature of 450 ^{0}C is affected by larger uncertainty because it was the result of calculating the suitable thickness of the helium gap between specimen capsule and inner rig wall. The irradiation samples with a

shape of flat tensile samples were 15 mm long, with a rectangular gauge section of 1.5 mm x 1.7 mm, and 8.5 mm in length, and the TEM disks were produced by cutting the heads of the samples. Small sample size ensured negligible temperature inhomogeneity under neutron irradiations. The irradiated materials were also characterized in terms of mechanical properties [40], positron annihilation spectroscopy [xx], small angle neutron spectroscopy [xx] and atom probe tomography whose results will be presented elsewhere in the nearest future.

2.2 TEM investigation

Specimens for the TEM investigation were prepared from the heads of flat mini tensile samples used for mechanical testing, whose results are recently reported in [40]. Due to their size and irradiation-induced activation, the heads were first cut-off from the gauge section in a hot-cell, and then polished mechanically with SiC paper to reduce the thickness to about 0.1 mm. At this reduced size, the activation level was low enough to work in a fume hood, where 3 mm and 1 mm disks were punched out. 1 mm disks were then glued on 3 mm platinum 0.5 mm slot TEM grids and then electro-chemically polished until perforation, alongside 3 mm disks, to complete the TEM specimen preparation. The composition of the electrolyte consisted of 5% per chloric acid in 95% methanol, temperature of -35°C to -25°C and a voltage of 40 V were applied.

2.3 OKMC modelling

In OKMC models, the evolution of an alloy under irradiation is described stochastically, with events implementing the migration and interaction of diffusing species; these are point defects or complexes involving point defects and solutes, e.g., vacancy-solute clusters. Parameters for the properties of vacancies and self-interstitial clusters were proposed in past works addressing increasingly complex alloys, as detailed in [29-31]. The work of Chiapetto et al. in Ref.[30] considered the Fe-C-NiMn alloy, while the work in Ref [31] considered Fe-C-Cr alloys. The effect of all alloying elements was accounted for in a ‘grey alloy’ approximation, i.e. their effect was translated into a change of the value of the parameters that define the mobility and stability of point defects and their clusters, as a function of the nominal composition. In this work, the model proposed in [37] is used. The main and crucial addition compared to works [29-31] concerns the explicit treatment and redistribution of solute atoms of different chemical nature during irradiation. Therefore, the Fe-C-Cr-NiSiP system is directly addressed, including explicitly all the alloying elements of steels used in nuclear applications that are known to produce nano-sized solute-rich clusters. Key reactions in our OKMC model are the dragging of solute atoms by single point-defects (as parameterized with DFT calculations), and the binding of solute atoms with small loops (also parameterized with DFT calculations). Only the Cr atoms remain treated in a grey alloy approximation, for simplicity, because of the concentrated compositions. The model is thus designed to describe the formation of vacancy clusters, SIA dislocation loops, and NiSiP-rich clusters under irradiation. By assumption, the latter form spontaneously in the model, as a consequence of radiation-induced segregation at immobilized SIA defects.

Our OKMC is fully described in Ref [37], for the specific application to Fe-C-CuNiMnSiP alloys, which is representative for Reactor Pressure Vessel (RPV) steels. The same model is here applied to Fe-C-Cr-NiSiP alloys, given the following adaptations:

- The effect of Cr is accounted for by changing the diffusion parameters of SIA defects. As derived in Ref. [41] and later on used in the OKMC model in Ref. [31], the attempt frequency for SIA migration is influenced by the Cr concentration.
- Parameters describing the interaction energies between Ni, Si or P solute atoms and single vacancy or single SIA defects, or small vacancy-solute clusters, are unchanged compared to Ref.[37]. These are crucial input parameters, derived for DFT calculations, that regulate atomic transport and the reduction of SIA defects diffusion. They thus regulate the seeding rate of SRC in the model.
- Some free parameters must be defined in the model, nevertheless. As explained in Ref.[37], the parameters regulating the thermal stability of SRC are not known with accuracy from DFT calculations. They are thus empirically determined, making simplifying assumptions. Two parameters need to be adapted for the specific application to Fe-C-Cr-NiSiP alloys: (a) the binding energy between single vacancies and big SRC is assumed to be a constant value denoted as $E_{bind}^{(V-SRC)}$. In Ref.[37], that parameter was chosen to be 0.6 eV, while in this work a lower value of 0.3 eV leads to more accurate predictions. This difference can be explained by the significant difference in the chemical composition, including the presence of Cr; (b) the binding energy between vacancy-solutes pairs and nucleated SRC is assumed to be another constant value denoted as $E_{bind}^{(VS-SRC)}$. In Ref.[37], we showed that the predictions of the OKMC model compare well with experimental evidence from atom probe tomography and small angle neutron scattering, if this parameter is chosen in a narrow range: $E_{bind}^{(VS-SRC)}$ = 0.7 to 0.9 eV. Similar values are used in this work.

Importantly, it is worth emphasizing that:

- The OKMC model assumes that all SIA defects have ½<111> Burger vectors, while it is known experimentally that a fraction of <100> loops is also observed [42]. This is especially pronounced for pure Fe, because 90% of the loops are <100> in this case. In Fe-9%Cr alloys, however, the observed fraction of <100> is reduced to 0.3.
- The model is in practice employed using simulation boxes that are orders of magnitude smaller than grains, with a size of approximately 30-50 nm size. Periodic boundary conditions emulate bulk conditions. It is thus conceptually forbidden to place a dislocation line in the box, or else the effective density of dislocation would be unrealistically high. For that reason, the model includes the sinking effect of dislocation lines, and equivalently the sinking effect of grain boundaries, via theoretical sinks strength formulas. Therefore, while sink strengths are in principle accounted for with realistic magnitudes, the model cannot describe heterogeneous distributions of defects, e.g. decoration or depleted zones.

3. Results and discussion

3.1 Microstructure of non-irradiated materials

TEM images of the non-irradiated model alloys and pure Fe in as-received condition are shown in Fig. 1. An upper panel presents a general view in the low magnification condition with grain boundaries visible, while the lower pane shows the appearance of dislocations. Pure Fe, Fe-9Cr, and Fe-9Cr-NiSiP alloys exhibit fully ferritic

microstructure. In pure Fe, dislocation lines are observed throughout the specimen together with spaced dislocation tangles. The average dislocation density is measured to be 1.18×10^{13} m^{-2}. Rarely, the dislocation loops were also observed in several areas of the specimen. These loops are homogeneously distributed over the studied area and their size was measured to be in the range 5 nm to 35 nm, while their density was calculated to be 5.39×10^{19} m^{-3}. Similar density and size of the loops was observed in the model alloys, and we suspect that these loops originate from the punching of the sample (material is too soft and therefore experiences plastic deformation, the softer the material – the higher the dislocation loop density). Given the very low density of the loops, it will be very easy to distinguish the irradiation-induced loops as will be shown below.

In Fe-9Cr alloy, the dislocation lines were regularly observed throughout the specimen with the density of about 1.62×10^{13} m^{-2}, see a lower pane on Fig. 1. Seldom dislocation loops were also observed in this specimen, the density was calculated to be 1.25×10^{17} m^{-3}, thus the density of dislocation loops is lower in Fe-9Cr than in pure Fe.

The microstructure of the Fe-9Cr-NiSiP alloy consists mainly of dislocations and grain boundaries. The dislocation lines are observed throughout the specimen. Only few dislocation loops are found in various examined areas presented, such as shown in the lower pane of Fig. 1. Overall, it was noticed that a higher concentration of dislocations appears near the grain boundaries, where some dislocation networks are also observed.

The observation of loops and tangled dislocations is not expected in the material in the reference state. It is possible that these microstructural features occur either as a consequence of plastic deformation during the sample preparation at room temperature, or they were created during the alloys manufacturing as a consequence of insufficient tempering. Additional investigation is needed to clarify these possibilities. Because of that, one has to keep in mind that similar features may also appear in the TEM samples which were neutron irradiated. However, as will be shown, the density of the irradiation induced defects is much higher and therefore it is very easy to reveal the impact of the neutron irradiation.

Given that the thermal stability of the microstructure of the model alloys is not known, we have annealed the materials at 450°C for the same duration as the neutron irradiation lasted (i.e. six weeks). Several TEM samples were inspected using the thermally aged alloys. The images showing the low and high magnification conditions are presented in Fig. 2, on the upper and lower panes, respectively. Thermal aging did not cause the significant change of the microstructure in both alloys. Thermal aging caused a slight reduction of dislocation density by approximately a factor of two in each material. No obvious change in the grain size was seen. The dislocation loops, seen in non-aged materials, were no longer observed after the thermal ageing. This suggests that the sample preparation was not the cause of the observation of the loops. Likely, the loops were due to the non-sufficient tempering after the manufacturing.

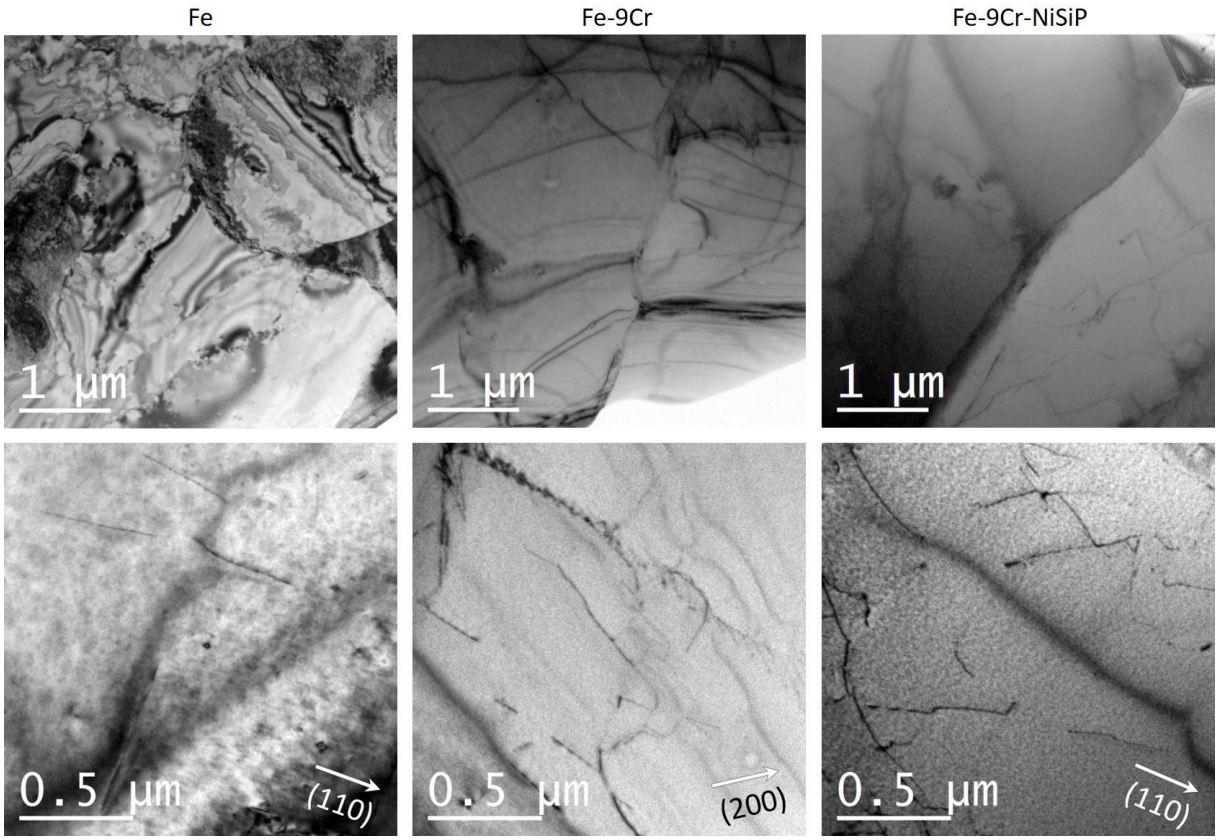

Fig. 1. Low magnification BF TEM images showing the microstructure of pure Fe, Fe-9Cr and Fe-9Cr-NiSiP materials. Upper pane shows the typical appearance of grain interiors/boundaries, while lower pane shows the appearance of dislocations in these materials.

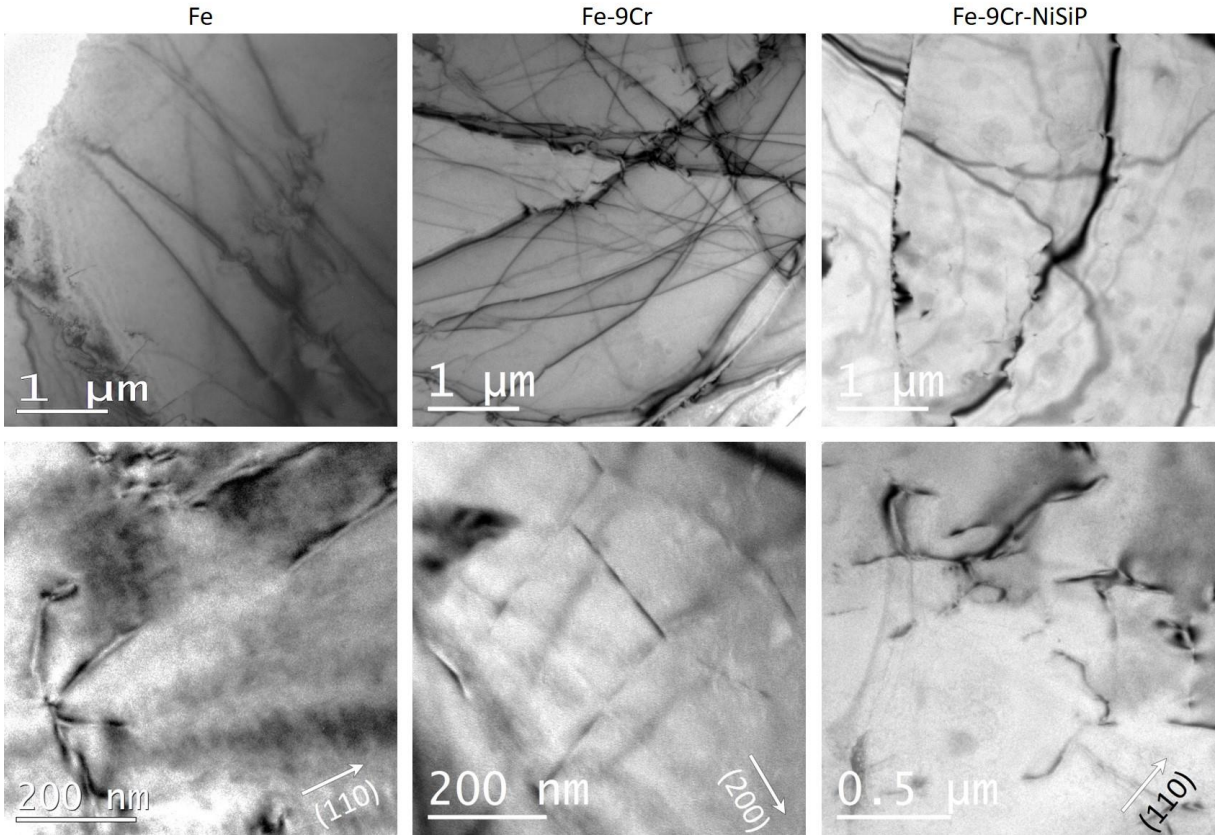

Fig. 2. Impact of the thermal annealing on the microstructure of pure Fe, Fe-9Cr and Fe-9Cr-NiSiP materials. Upper and lower panes show the low and high magnification images, respectively.

3.2 Microstructure of neutron irradiated materials

3.2.1 Microstructure after irradiation at 450°C

This section reports TEM investigations of the neutron irradiated materials, irradiated at 450°C to a dose of 0.11 dpa. Due to the activation induced by neutron irradiation, the operation time with the samples was limited. Thus, the focus was put on understanding of the effect of solutes and irradiation temperature to the dislocation loop size/spatial distribution without in-depth analysis of the Burgers vector and nature of the loops (i.e. interstitial/vacancy).

The dislocation density has decreased in both pure Fe and model alloys in comparison with the as-received sample. In Fe and Fe-9Cr the decrease was smaller (~24%) then in Fe-9Cr-NiSiP (~34%). Images of the microstructure after neutron irradiation are shown in Fig. 3.

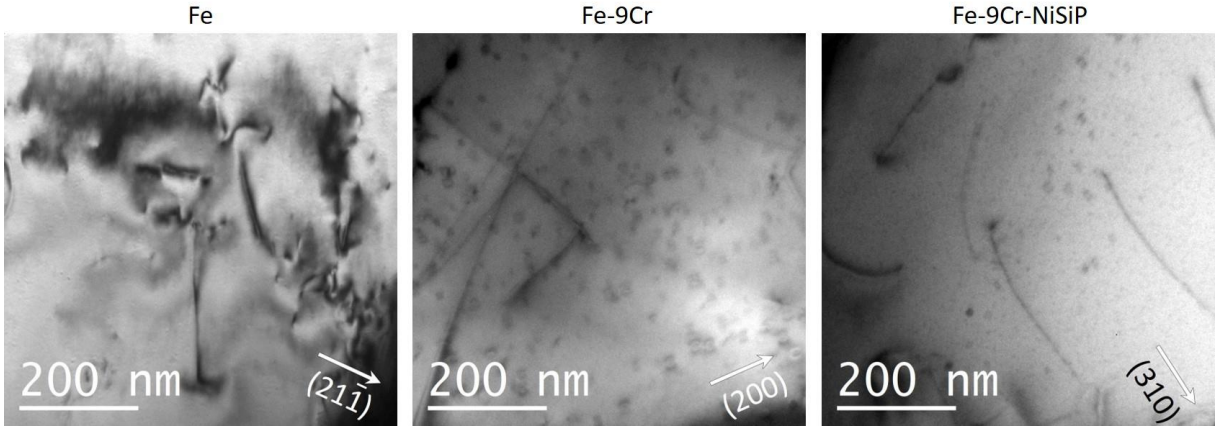

Fig. 3. Images of the dislocation structures in pure Fe, Fe-9Cr and Fe-9Cr-NiSiP alloys after neutron irradiation at 450°C.

Table 2. Summary on dislocation line and dislocation loop density observed in the as-received, aged and irradiated state. The units for dislocation density are $1/m^2$, and dislocation loop density is $1/m^3$.

Material	Dislocation density, as received	Dislocation density, aged at 450°C	Dislocation density, irradiated at 450°C	Dislocation loop density, irradiated at 450°C
Fe	1.18E+13	7.54E+12	9.09E+12	1.32E+20
Fe-9Cr	1.62E+13	1.02E+13	1.22E+13	1.39E+21
Fe-9Cr-NiSiP	1.39E+13	7.92E+12	9.2E+12	1.75E+22

Dislocation loops are main features observed by TEM that were induced by the neutron irradiation. The attempts to detect voids were applied to all inspected samples, but without success as non were observed. Dislocation loops were observed in all the irradiated materials. Representative TEM images of the loops are provided in Fig. 4. The

dislocation loops were observed inside the grain interior to be homogeneously distributed and also some fraction of the loops was observed along the dislocation lines.

In pure Fe, the dislocation loops were rather large, up to 80 nm in size and have clearly pronounced coffee bean shapes and being mostly homogeneously distributed, see Fig. 5. This microstructure resembles the one observed by Horton et al. [43], where such loops were identified to be of a_0<100> type in neutron irradiated pure Fe at 300-450°C. Dislocation loops in pure Fe under neutron irradiation at 300C at 0.1 dpa were also observed by Meslin et al.[8] with a density of 10^{21} m^{-3} with the size below 10 nm. The loops were distributed homogeneously in the matrix, though in some cases dislocation decoration was also observed. The Burgers vector of the majority of the loops was determined to be a_0<100>. The low size and relatively high density observed by Meslin [8] is clearly explained by the irradiation temperature, while our observations are in good qualitative and quantitative agreement with the observations of Horton [43] for the irradiation temperature of 450°C.

In model alloys dislocation loops size was smaller and the decoration of dislocation lines was observed more often. The examples of the loops decorating dislocation lines in Fe-9Cr and Fe-9Cr-NiSiP alloys are presented in Fig. 6 and Fig. 7, respectively.

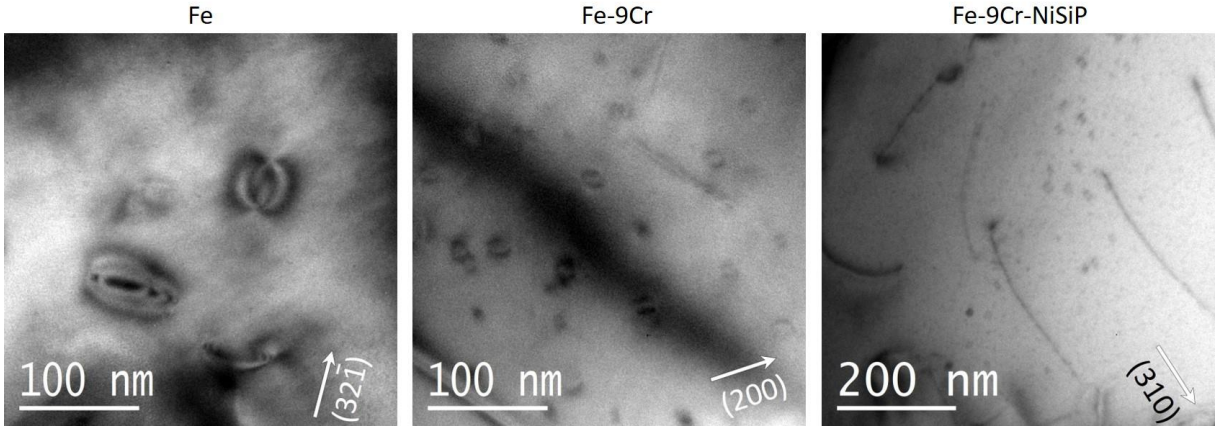

Fig. 4. Representative TEM images of the irradiation induced dislocation loops at Tirr=450°C.

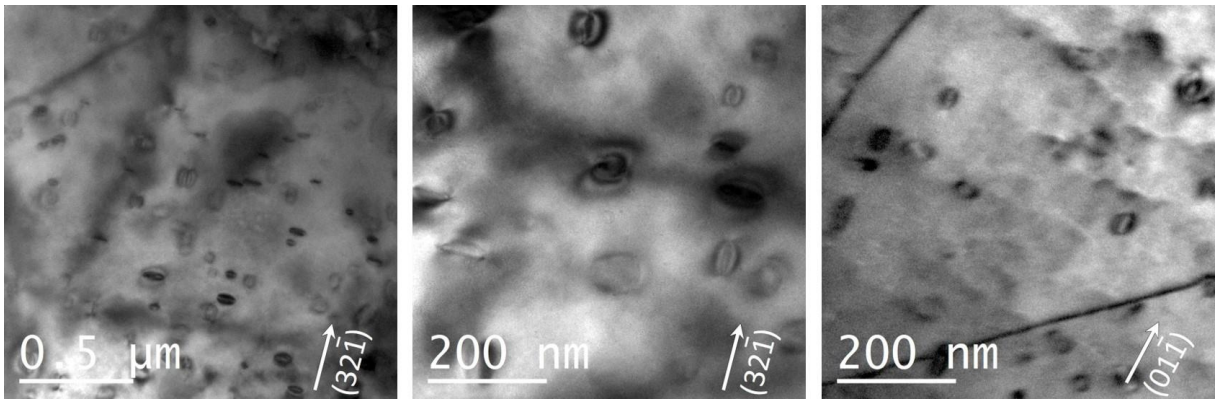

Fig. 5. TEM images of the irradiated pure Fe. Dislocation loops and dislocations lines (right hand image) are shown.

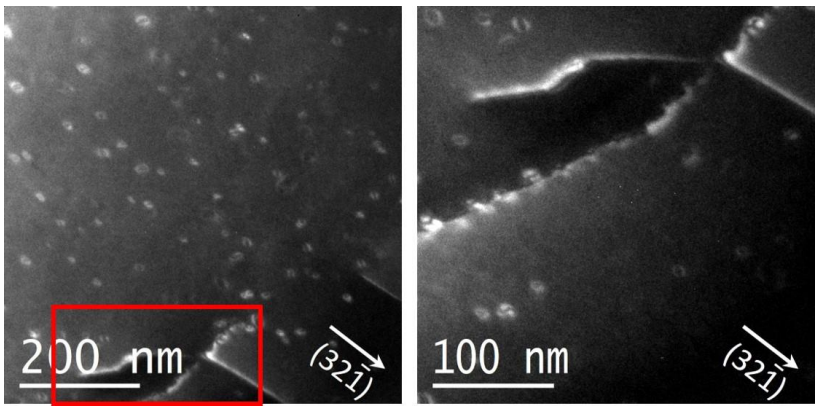

Fig. 6. Dark field TEM images of the irradiated Fe-9Cr alloy. The left hand image shows that low magnificent image with loops and dislocation line, decorated by the loops. The right hand side shows the higher magnification image (of red rectangular on the left figure) of the loops near the dislocation line.

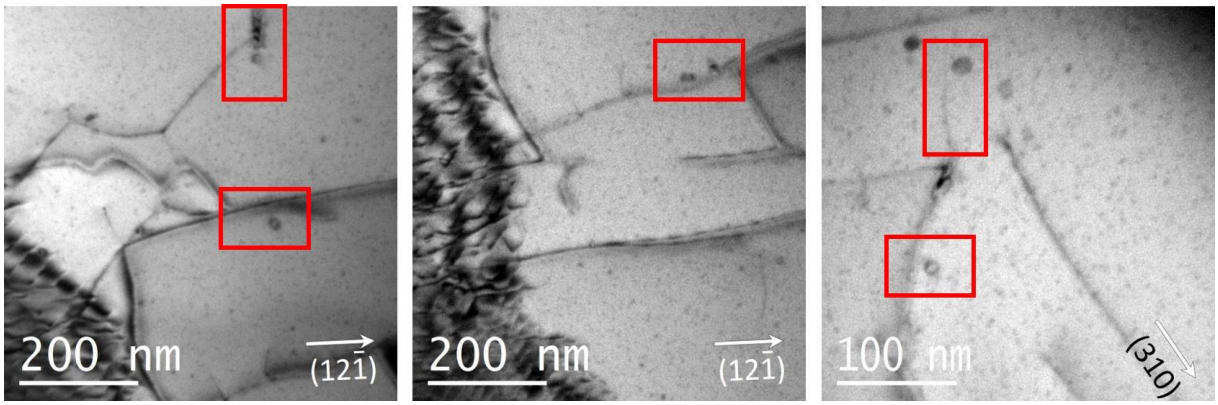

Fig. 7. TEM images of the irradiated Fe-9Cr-NiSiP alloy. The images show the presence of the irradiation induced loops nearby the dislocation lines. The areas containing large loops located in the vicinity of the dislocation lines are highlighted by red rectangulars.

The average loop size was found to be the smallest in Fe-9Cr-NiSiP, but at the same time it has larger loop density in comparison with both pure Fe and Fe-9Cr. In fact, in the Fe9Cr and Fe9Cr-NiSiP alloys, the loops have bi-modal size distribution. Small and numerous dislocation loops were distributed homogeneously, while few large loops were observed to decorate dislocation lines, as shown on Fig. 6-.7 In general, the fraction of the dislocation loops decorating dislocation lines is rather small. Still, the association of large loops with dislocation lines was detected in almost all of the investigated areas and samples.

The size distribution of dislocation loops and density is shown in Fig. 8. In pure Fe the size of dislocation loops sizes a ranges from 10 to 80 nm, with an average size of about 45 nm. The mean size of the loops is 3 nm and 15 nm in the NiSiP-doped and pure 9Cr alloy, respectively. As it follows from Fig. 8, the lowest dislocation density is obtained in pure Fe being 10^{20} m^{-3}, while it exceeds 10^{22} m^{-3} in the Fe-9Cr-NiSiP alloy.

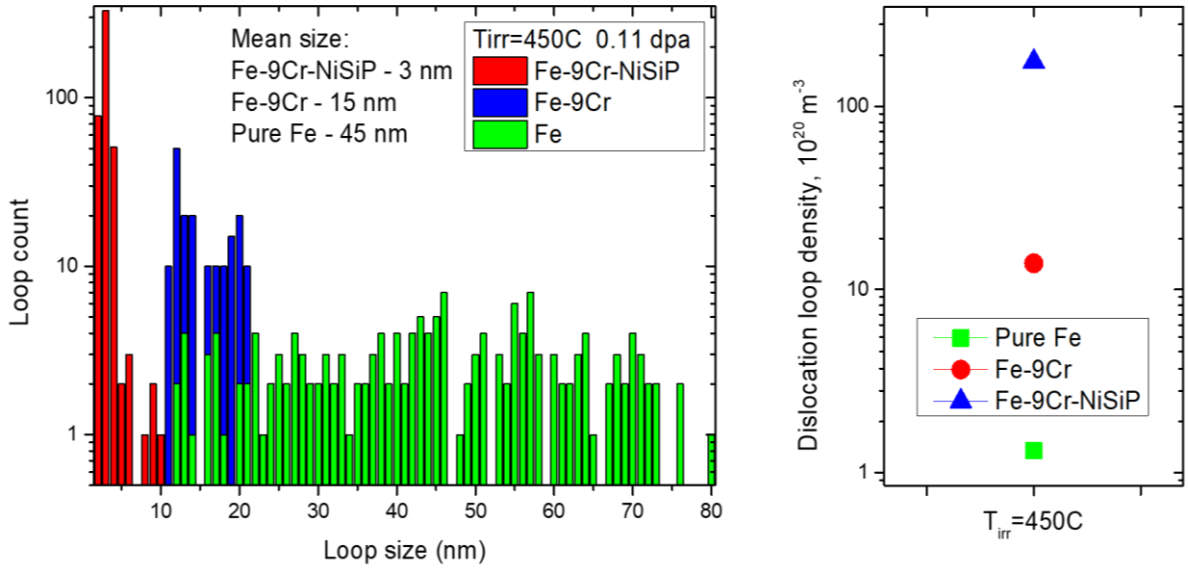

Fig. 8. The size distribution of dislocation loops and density obtained by TEM after irradiation at T_{irr}=450°C.

3.2.2 Microstructure after irradiation at 290°C

In this section, we present the results of TEM investigation of materials irradiated at 290°C to 0.11 dpa. Pure Fe samples were not added for the irradiation at this temperature, thus we limit the results to the alloys. Just as in the case of Tirr=450°C, the attempts to find voids were not successful. The dislocation density after the irradiation did not change considerably (within the standard deviation) in both alloys. The only remarkable features of the microstructure induced by the irradiation were the dislocation loops.

Fig. 9 shows the microstructure of the Fe-9Cr alloy. In this material, the spatial distribution of the loops depended on the local dislocation density. In the regions with high dislocation density (see Fig. 9a,b), most of the loops were found to decorate the dislocation lines. In the regions with medium dislocation density, the loops are mostly homogeneously distributed such as shown for two separate areas in Fig. 9c and 9d. Close look at the loops in the different regions, including the loops located closely to the dislocation lines (see Fig. 9b), revealed that the size distribution of the loops is the unimodal, while it is bi-modal at Tirr=450°C. The density and mean size of the loops with the homogeneous spatial distribution is estimated to be 8×10^{19} m^{-3} and 4 nm, respectively.

Fig. 10 shows the microstructure of the Fe-9Cr-NiSiP alloy. As was noticed above, the average dislocation density did not change after the irradiation, however, the dislocations loops are not well visible in the case of lower magnification images, see Fig. 10a and 10b. At increased magnification, it is becoming evident that some dislocation lines have irregular pattern which is likely to be attributed to the decoration by the dislocation loops, see examples of two different areas on Fig. 10c and Fig. 10d. Rare standalone loops with the size of 5-8 nm could also be observed on Fig. 9c. From the limited analysis of the size and spacing of the dislocation loops, we could derive that their mean spacing in clusters along the dislocation lines lies within the range of 10-20 nm on average and their size is in the range of 1.5-2.5 nm on average.

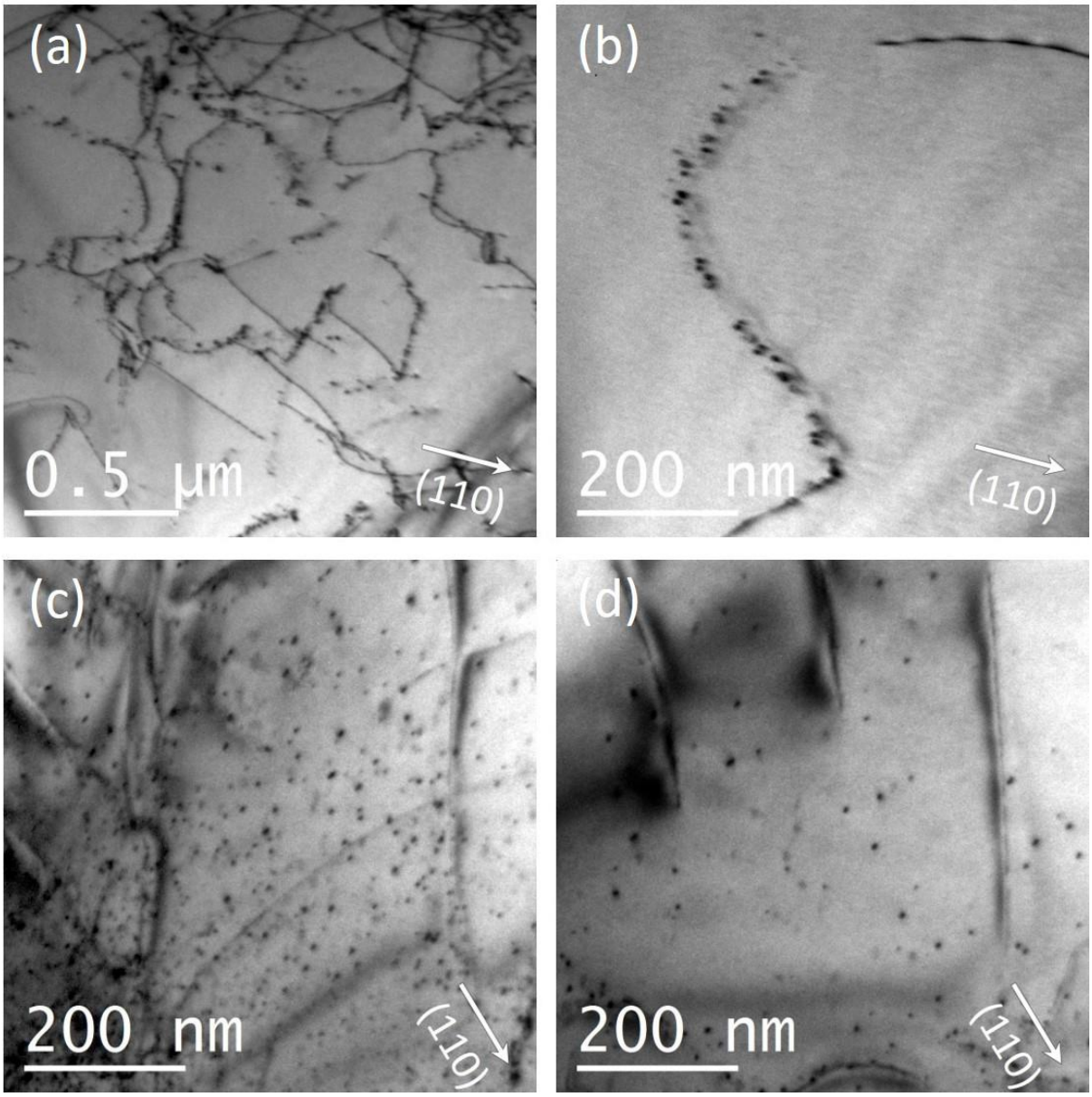

Fig. 9. TEM images of the irradiation induced microstructure in Fe-9Cr at T_{irr}=290°C. (a) general overview of the dislocation microstructure in the region where the decoration by loops dominates; (b) a dislocation line decorated with loops; (b), (c) micrographs showing the regions where loops are mostly homogeneously distributed.

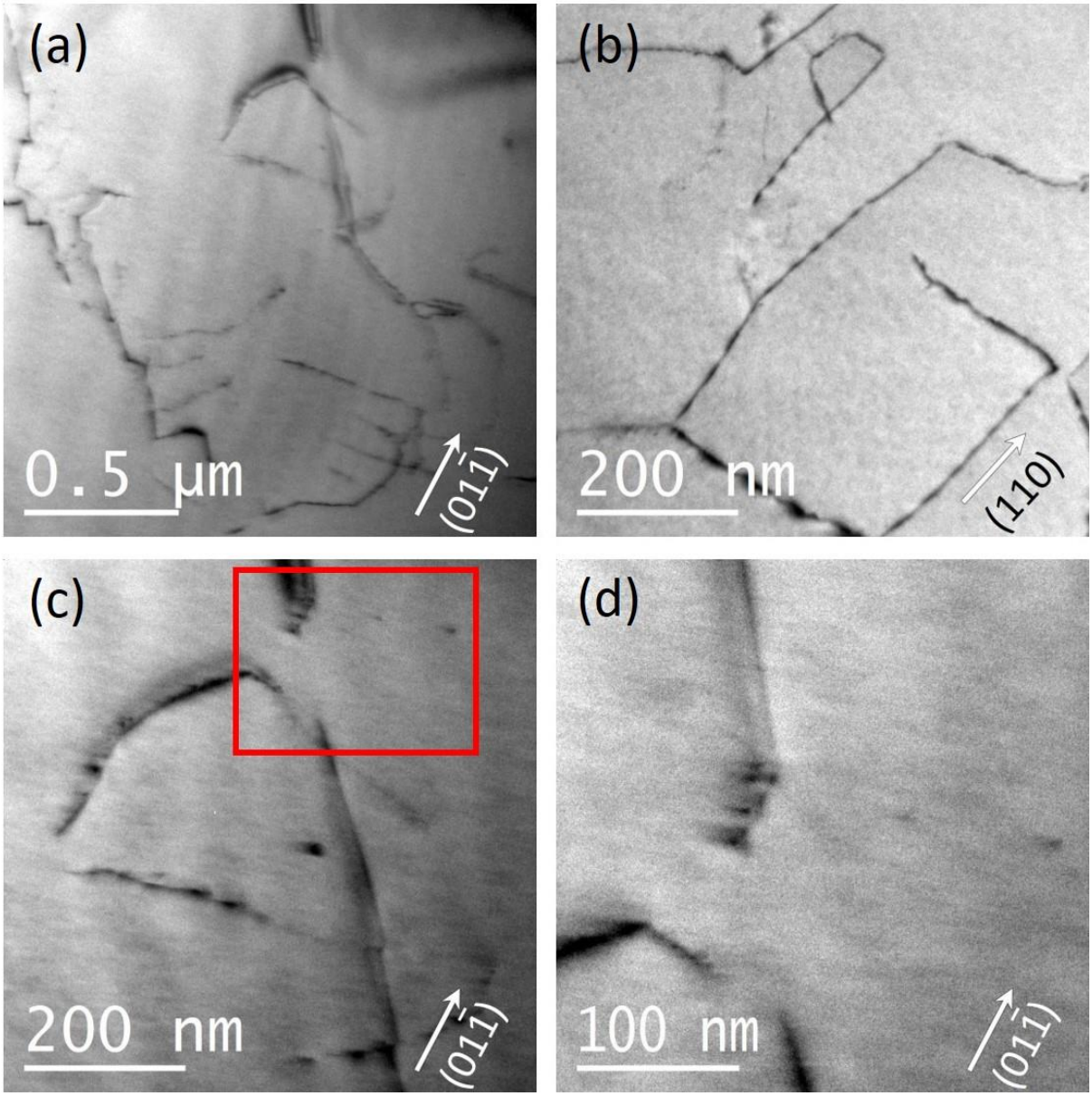

Fig. 10. TEM images of the irradiation induced microstructure in Fe-9Cr-NiSiP at T_{irr}=290°C. (a), (b) typical view of the dislocation microstructure, no isolated large loops are observed; (c) TEM micrograph showing dislocation line decorated by the loops and rare standalone loops; (d) higher magnification image showing a zoomed region of fig. (c) to demonstrate that the distortion of the dislocation line pattern is related to the decoration by the loops.

Before we proceed to presenting OKMC results, let us summarize the TEM investigations. Dislocation loops are the main feature induced by neutron irradiation. They were clearly observed by TEM in all irradiated samples studied here. Under the irradiation at 450°C, the dislocation loops were homogeneously distributed all over the investigated area in pure Fe, Fe-9Cr and Fe-9Cr-NiSiP. Small fraction of the loops was observed to decorate the dislocation lines in the alloys. The dislocation loop density was found to be the highest in Fe-9Cr-NiSiP, but at the same time it has the smallest average loop size in comparison with both pure Fe and Fe-9Cr. Evidently, an addition of Ni, Si and P reduces the size of the irradiation-induced loops and strongly increases their number density.

Under irradiation at 290°C, the numerous small loops were observed in the Fe-9Cr alloy, where regions with pronounced decoration of dislocation lines by the loops were regularly presented. The regions with homogeneous

loop distributions were observed often as well. It seems that high dislocation density provokes segregation of the loops and does allow to establish homogenous loop distribution pattern. In the case of Fe-9Cr-NiSiP, the majority of the observed loops was found to decorate dislocation lines.

3.3 OKMC modeling:

As a first step, the OKMC model is validated while performing simulations of irradiation experiments in Fe-C-Cr-NiSiP alloys at 290°C. The content of Cr varies between 2.5at%, 5at% and 9 at%, while the content in Ni, Si and P remains very similar in all cases, to comply with the available experimental data. Overall, the total content of Ni, Si and P solutes varies between 0.1 at% and 0.15 at%, which is an intermediate concentration between the G385 (Fe-9Cr) and G389 (Fe-9Cr-NiSiP) compositions listed above in Table 1. The model assumes $E_{bind}^{(V-SRC)}$= 0.3 eV and $E_{bind}^{(VS-SRC)}$= 0.8 eV, following the description of the model provided in Section 2. Consistently with the microstructure characterization of these materials, the grain size is assumed to be 50 µm for the Fe-2.5%Cr alloy, 35 µm for the Fe-5%Cr alloy and 20 µm for the Fe-9%Cr alloy. The Carbon content was taken to be 20 appm and the dislocation density to be $6 \cdot 10^{13}$ m^{-2} in all cases. The OKMC results are compared to the experimental data in Fig. 11, see figure caption for details of the experimental works. The comparison provided in Fig. 11 demonstrate the following:

- Both the number density and the average size of the SRCs, as predicted by the OKMC model, fall in the same range as observed experimentally by APT.
- The predicted number density of SIA loops falls in the same range as reported by the TEM (as dislocation loops). However, the OKMC model significantly underestimates the average size of those loops.

Therefore, the OKMC model is adequately parameterized to predict the kinetics of formation of SRC, but apparently has certain limitations at predicting the population of SIA loops with accuracy.

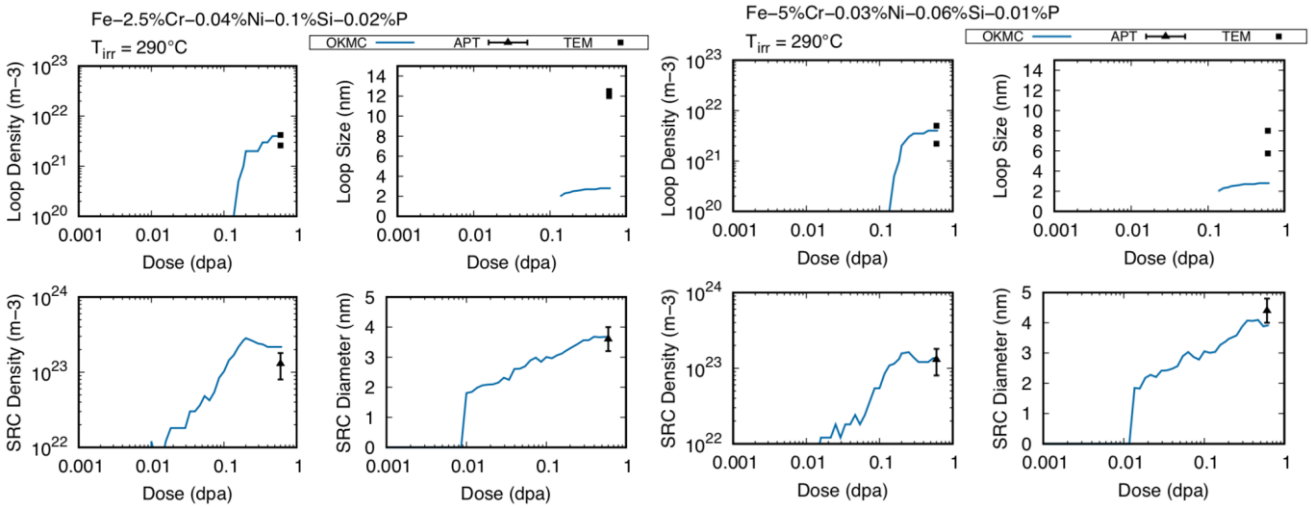

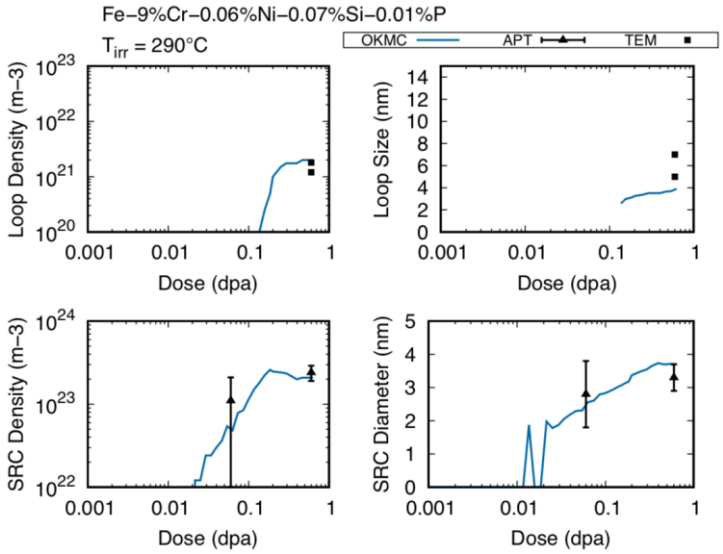

Fig. 11. Prediction of the OKMC model compared to experimental evidence, for three different model alloys irradiated at 290°C. The TEM data (number density and average size of SIA loops) is taken from Ref.[28, 42] and the APT data (number density and average size of SRC) is taken from Ref.[44].

Next, the model was applied to simulate the irradiation experiments at 290°C and 450°C for the materials studied in this work, adopting the chemical composition as listed in Table 1. Again, we take $E_{bind}^{(V-SRC)}$= 0.3 eV and $E_{bind}^{(VS-SRC)}$= 0.8 eV. Consistently with the microstructural characterization of these materials, the grain size is taken to be 20 µm. The Carbon content was assumed to be 100 appm (as suggested by APT measurements [45], the detailed presentation of the APT results will be done in a separate work) and the dislocation density was assumed to be 10^{13} m^{-2} in all cases (as listed above in Table 1). In the case of pure Fe and Fe-9Cr materials, APT analysis revealed no presence of SRC, and our OKMC model yielded to the same conclusion. Nevertheless, in the case of the Fe-9Cr-NiSiP material, APT revealed the presence of relatively large solute clusters. As shown in Fig. 12, the OKMC model results to a similar prediction. This result highlights that the OKMC model delivers a realistic prediction of the formation of the SRCs under neutron irradiation at 450°C.

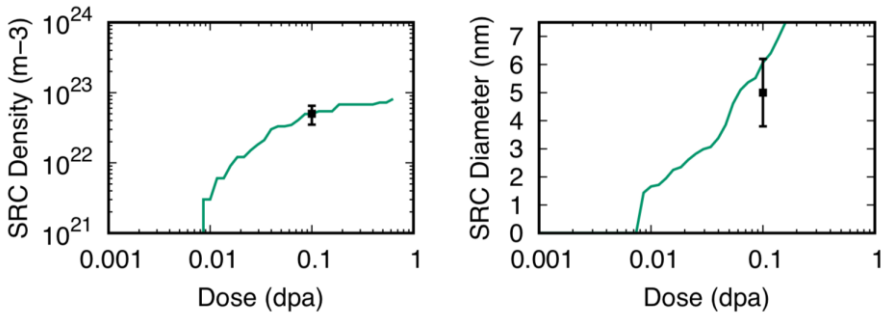

Fig. 12. Prediction of the OKMC model compared to experimental evidence by APT [N], for the irradiation of the Fe-9Cr-NiSiP material at 450°C.

When analysing the results in terms of SIA defects, it turns out that the population of the TEM-visible loops is not satisfactorily predicted by the OKMC model. In Fig. 13, we plotted the size distribution of SIA defects that are predicted by the model, for the three materials and the two irradiation temperatures. We can see that the OKMC

model systematically underestimates the population of SIA defects in terms of number density and average size for the case of T_{irr}=450°C when compared with the experimental data. In particular, the OKMC model predicts strong reduction of the loop density when the irradiation temperature is increased from 300°C up to 450°C. The following cross-comparison of the OKMC prediction and TEM results can be made:

- At 290°C, in all three materials, the OKMC model predicts that a number density ≈ 10^{22} m^{-3} of loops should form, which big enough to be visible to the TEM (size > 2.5 nm). Such loops are observed experimentally (see Fig. 9 and Fig. 10 in section 3.2.2), but they are mostly found along dislocation lines. As explained above, the OKMC model deals with the effective sink strength and does not contain dislocation lines/grain boundaries as objects for the sake of the computational efficiency. Hence, the OKMC model in the present state does not follow spatial heterogeneity of the defects and we can not extract the predicted linear density of the loops aggregated around the sinks. Taking the materials irradiated at 290°C, the density of the loops decorating the dislocations can be reliably estimated by TEM only for the Fe-9Cr, where the loop density is estimated (as a lower bound of the measurements) to be 8×10^{19} m^{-3}. Another important feature of the OKMC model is its prediction of the impact of Cr on the significant reduction of the loop size, see results shown in Fig. 13. The addition of NI-Si-P reduces the loop size even further. This effect is well in line with the experimental observations at T_{irr}=450°C, as pure Fe has the biggest loops, Fe-9Cr – medium size and Fe-9Cr-NiSiP contains the smallest ones.
- At 450°C, the model predicts that the number density of TEM-visible loops would be lower than at 290°C, by at least one or two orders of magnitudes. This is clearly in contradiction with the experimental evidence. Likewise, the model does not predict any significant difference in the SIA defects population between pure Fe and the model alloys.

Let us discuss possible physical and methodological reasons for the reported above discrepancy between the OKMC and experimental data. One of the main fundamental elements of the utilized OKMC model is the assumption that all SIA defects have $a_0/2$<111> Burger vectors, while a_0<100> loops are neglected. This assumption was supported by the TEM observations done earlier in [42], and also in this work the screening g×b analysis has confirmed that most of the loops formed in the alloys are of $a_0/2$<111> type. In the case of pure Fe, the loops were indeed mostly of a_0<100> type. Nevertheless, the analysis of the OKMC predictions performed in this work suggests that the assumption on the exclusive presence of $a_0/2$<111> loops does not accurately represents the actual processes taking place under irradiation at high temperature i.e. at 450°C as studied here. The analysis of the OKMC results presented in this work therefore suggests that a population of <100> SIA defects probably forms, even if they are not resolved by the TEM techniques. Considering that these <100>-type defects are much less mobile than ½ <111> defects, they likely play a significant role on the nucleation of TEM-visible loops.

The balance and ratio of a_0<100> and $a_0/2$<111> loops formed in Fe and Fe-Cr alloys is the subject that has been addressed by theoretical studies by several teams [46-48]. Three main hypotheses were put forward to explain the experimental evidence showing that the fraction of the a_0<100> loops increases with the irradiation temperature in pure Fe [49-51], while in the Fe-Cr alloys this is not the case. The first one was proposed based on the molecular dynamics (MD) simulations done by Wirth and Marian [47] and Terentyev et al [52], who hypothesized that a_0<100> loops are formed in direct reactions between two a0/2<111> loops. This hypothesis was then confirmed by the rigorous AKMC simulations confirming that the reaction proceeds with certain energy barrier which is of the order of 1 eV [48], explaining why the complete transition was not observed at the MD timescale. The second

explanation was proposed by Dudarev et al.[53], who argued that the self-energy of the a_0<100> loops becomes lower than that of $a_0/2$<111> due to the anomalous variation of the elastic constants at high temperature close to the BCC-FCC transition point. Finally, the third hypothesis was placed by Terentyev et al. [54], who studied the nucleation of the a_0<100> loops by collection of individual self-interstitial defects and demonstrated that vibrational entropy stabilizes the self-energy of the nucleus of a_0<100> loops.

Considering the applied here OKMC model, the introduction of the formation of a_0<100> loops via the nucleation or via reactions between two $a_0/2$<111> loops, as was applied by Terentyev and Bragado [55] to simulate electron irradiation, seems to be the natural next step for the development of the model. Besides the role played by the dislocation loops with two different Burgers vectors, the present model does not incorporate the sinks as direct objects, instead they are introduced via the cross-section reactions for the mobile defects according to the well-established theoretical framework. The present experimental observations show clearly that depending on the irradiation temperature and presence of Ni-Si-P alloying elements weak or strong decoration of the loops at dislocation lines and/or grain boundaries occurs. Correspondingly, the reproduction of such experimental evidence requires inclusion of dislocations as implicit OKMC objects. However, for the studied here materials, the density of the dislocations is rather low (compared to a typical dimension of the OKMC box) which implies that much larger simulation crystals (with inevitable impact on the computational efficiency) must be considered. The incorporation of different reaction channels and multiple family of the dislocation loops together with direct placement of sinks will require further development of the OKMC code to enable efficient integration while taking care of the mass transport, which is critical to observe the formation of SRCs.

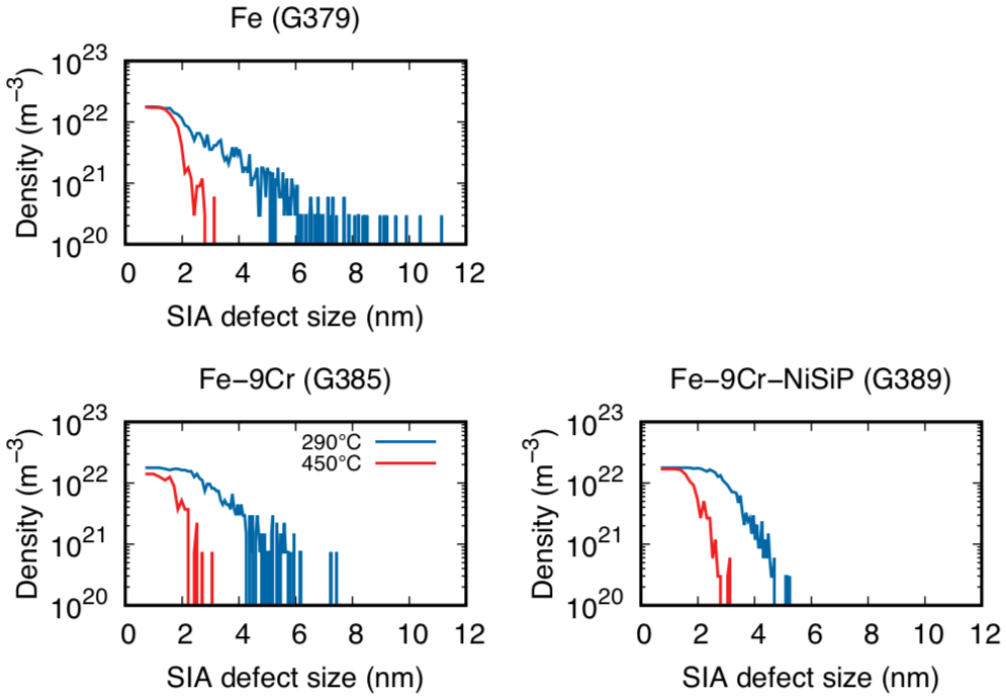

Fig. 13. Prediction of the OKMC model for the population of SIA defects, when irradiating different materials up to 0.1 dpa at 290°C and 450°C.

4. Summary and conclusive remarks

TEM investigation of non-irradiated and neutron irradiated high Cr F/M alloys and steels was performed. The focus was given on the assessment of the dislocation loop distribution (size and density) as a function of irradiation temperature and chemical composition of investigated alloys. Several Fe-Cr model alloys with different chemical composition were neutron irradiated by utilizing the BR2 reactor at temperatures of 290 °C and 450°C, up to the dose of about 0.11 dpa. Besides the neutron irradiation, the high temperature annealing was performed at 450°C in order to study an interplay of thermal ageing and irradiation to the defect formation.

Dislocation loops were discovered to be the main features induced by the neutron irradiation. They were clearly observed by TEM in all irradiated materials. In the case of 450°C irradiation, the dislocation loops were homogeneously distributed all over the investigated area in pure Fe, Fe-9Cr and Fe-9Cr-NiSiP. The average loop size was observed to be much smaller in Fe-9Cr-NiSiP than in the case of pure Fe and Fe-9Cr. On the contrary, Fe-9Cr-NiSiP has the larger loop density in comparison with both pure Fe and Fe-9Cr. Evidently, an addition of Ni-Si-P elements, rather than the increase of Cr concentration, reduces the size of loops and increases their number density. Under irradiation at 290°C, the numerous small loops were observed in the Fe-9Cr alloy, where regions with pronounced decoration of dislocation lines by the loops were regularly presented. The regions with homogeneous loop distributions were observed often as well. In the case of Fe-9Cr-NiSiP, the vast majority of the observed loops was found to decorate the dislocation lines. The areal density of the loops observed in the Fe-9Cr-NiSiP was evidently higher than in Fe-9Cr, which might imply that a large fraction of small dislocation loops (interstitial clusters) is present in the matrix but is invisible to TEM due to small size.

To rationalize the experimental observations and possibility substantiate the hypothesis on the presence of TEM-invisible microstructure, we have carried out OKMC simulations employing the model which accounts simultaneously for the presence of solid solution (as gray alloy) and minor alloying by Ni-Si-P [37].

The OKMC model successfully predicted the formation of NiSiP-rich clusters which are also observed in the experiments by APT, under the neutron irradiation at both 290°C and 450°C. The predicted size and density of SRCs were in good agreement with the experimental data. However, the predicted microstructure in terms of SIA loops is found to deviate from the experimental evidence obtained here. As discussed above, the two limitations of the utilized OKMC model could explain the deviation, namely: (i) lack of dislocations/grain boundaries as direct sinks present in the model which would offer decoration and heterogeneous loop distribution; (ii) single family of the dislocation loops instead of two types of the loops with Burgers vector of $a_0/2<111>$ and $a_0<100>$ types, correspondingly experiencing different migration energy barrier.

Acknowledgements

This work has been carried out within the framework of the EUROfusion Consortium and has received funding from the Euratom research and training programme 2014-2020 under grant agreement No 633053. The views and opinions expressed herein do not necessarily reflect those of the European Commission.

Data availability

The raw/processed data required to reproduce these findings cannot be shared at this time as the data also forms part of an ongoing study.

References

[1] S.J. Zinkle, J.T. Busby, Structural materials for fission & fusion energy, Materials today 12 (2009).
[2] G.S. Was, Fundamentals of Radiation Materials Science, Springer, New York, 2007.
[3] W. Hoffelner, Damage assessment in structural metallic materials for advanced nuclear plants, J Mater Sci 45(9) (2010) 2247-2257.
[4] G.R. Odette, On the dominant mechanism of irradiation embrittlement of reactor pressure-vessel steels, Scripta Metall Mater 17(10) (1983) 1183-1188.
[5] G.R. Odette, G.E. Lucas, Embrittlement of nuclear reactor pressure vessels, Journal of the Minerals Metals & Materials Society 53(7) (2001) 18-22.
[6] G.R. Odette, B.D. Wirth, A computational microscopy study of nanostructural evolution in irradiated pressure vessel steels, Journal of Nuclear Materials 251 (1997) 157-171.
[7] C.A. English, W.J. Phythian, R.J. McElroy, Microstructure and modelling of RPV embrittlement, Microstructure Evolution during Irradiation 439 (1997) 471-482.
[8] E. Meslin, M. Lambrecht, M. Hernandez-Mayoral, F. Bergner, L. Malerba, P. Pareige, B. Radiguet, A. Barbu, D. Gomez-Briceno, A. Ulbricht, A. Almazouzi, Characterization of neutron-irradiated ferritic model alloys and a RPV steel from combined APT, SANS, TEM and PAS analyses, Journal of Nuclear Materials 406(1) (2010) 73-83.
[9] C. Pareige, M. Roussel, S. Novy, V. Kuksenko, P. Olsson, C. Domain, P. Pareige, Kinetic study of phase transformation in a highly concentrated Fe-Cr alloy: Monte Carlo simulation versus experiments, Acta Materialia 59(6) (2011) 2404-2411.
[10] F. Bergner, C. Pareige, V. Kuksenko, L. Malerba, P. Pareige, A. Ulbricht, A. Wagner, Critical assessment of Cr-rich precipitates in neutron-irradiated Fe-12 at%Cr: Comparison of SANS and APT, Journal of Nuclear Materials 442(1-3) (2013) 463-469.
[11] V. Kuksenko, C. Pareige, C. Genevois, P. Pareige, Characterisation of Cr, Si and P distribution at dislocations and grain-boundaries in neutron irradiated Fe-Cr model alloys of low purity, Journal of Nuclear Materials 434(1-3) (2013) 49-55.
[12] Z. Lu, R. Faulkner, G. Was, B. Wirth, Irradiation-induced grain boundary chromium microchemistry in high alloy ferritic steels, Scripta Materialia 58 (2008) 878-881.
[13] T. Toyama, A. Kuramoto, Y. Nagai, K. Inoue, Y. Nozawa, Y. Shimizu, Y. Matsukawa, M. Hasegawa, M. Valo, Effects of post-irradiation annealing and re-irradiation on microstructure in surveillance test specimens of the Loviisa-1 reactor studied by atom probe tomography and positron annihilation, Journal of Nuclear Materials 449(1-3) (2014) 207-212.
[14] B. Radiguet, A. Etienne, P. Pareige, X. Sauvage, R. Valiev, Irradiation behavior of nanostructured 316 austenitic stainless steel, J Mater Sci 43(23-24) (2008) 7338-7343.
[15] M.K. Miller, Atom probe tomography characterization of solute segregation to dislocations and interfaces, J Mater Sci 41(23) (2006) 7808-7813.
[16] M.G. Burke, M. Watanabe, D.B. Williams, J.M. Hyde, Quantitative characterization of nanoprecipitates in irradiated low-alloy steels: advances in the application of FEG-STEM quantitative microanalysis to real materials, J Mater Sci 41(14) (2006) 4512-4522.
[17] F. Bergner, C. Pareige, M. Hernandez-Mayoral, L. Malerba, C. Heintze, Application of a three-feature dispersed-barrier hardening model to neutron-irradiated Fe-Cr model alloys, Journal of Nuclear Materials 448(1-3) (2014) 96-102.
[18] D. Terentyev, F. Bergner, Y.O. Osetsky, Cr segregation makes dislocation loops stronger, Acta Materialia 61 (2012) 1444-1453.

[19] E.E. Zhurkin, D. Terentyev, M. Hou, L. Malerba, G. Bonny, Metropolis Monte-Carlo simulation of segregation in Fe–Cr alloys, Journal of Nuclear Materials 417 (2011) 1082-1085.
[20] D. Terentyev, X. He, E. Zhurkin, A. Bakaev, Segregation of Cr at tilt grain boundaries in Fe-Cr alloys: A Metropolis Monte Carlo study, Journal of Nuclear Materials 408(2) (2011) 161-170.
[21] G. Bonny, D. Terentyev, A. Bakaev, E.E. Zhurkin, M. Hou, D. Van Neck, L. Malerba, On the thermal stability of late blooming phases in reactor pressure vessel steels: An atomistic study, Journal of Nuclear Materials 442 (2013) 282-291.
[22] Y.Y. Sun, Y.H. Zhao, B.J. Zhao, W.K. Yang, X.L. Li, H. Hou, Phase-field modeling of microstructure evolution of Cu-rich phase in Fe-Cu-Mn-Ni-Al quinary system coupled with thermodynamic databases, J Mater Sci 54(16) (2019) 11263-11278.
[23] D. Terentyev, N. Anento, A. Serra, Interaction of dislocations with carbon-decorated dislocation loops in bcc Fe: an atomistic study, J Phys-Condens Mat 24(45) (2012) 455402.
[24] S. Kotrechko, V. Dubinko, N. Stetsenko, D. Terentyev, X.F. He, M. Sorokin, Temperature dependence of irradiation hardening due to dislocation loops and precipitates in RPV steels and model alloys, Journal of Nuclear Materials 464 (2015) 6-15.
[25] G. Bonny, D. Terentyev, E.E. Zhurkin, L. Malerba, Monte Carlo study of decorated dislocation loops in FeNiMnCu model alloys, Journal of Nuclear Materials 452(1-3) (2014) 486-492.
[26] M.I. Pascuet, E. Martinez, G. Monnet, L. Malerba, Solute effects on edge dislocation pinning in complex alpha-Fe alloys, Journal of Nuclear Materials 494 (2017) 311-321.
[27] R. Ngayam-Happy, C.S. Becquart, C. Domain, First principle-based AKMC modelling of the formation and medium-term evolution of point defect and solute-rich clusters in a neutron irradiated complex Fe-CuMnNiSiP alloy representative of reactor pressure vessel steels, Journal of Nuclear Materials 440(1-3) (2013) 143-152.
[28] N. Castin, M.I. Pascuet, L. Messina, C. Domain, P. Olsson, R.C. Pasianot, L. Malerba, Advanced atomistic models for radiation damage in Fe-based alloys: Contributions and future perspectives from artificial neural networks, Computational Materials Science 148 (2018) 116-130.
[29] V. Jansson, L. Malerba, Simulation of the nanostructure evolution under irradiation in Fe-C alloys, Journal of Nuclear Materials 443(1-3) (2013) 274-285.
[30] M. Chiapetto, L. Malerba, C.S. Becquart, Nanostructure evolution under irradiation in FeMnNi alloys: A "grey alloy" object kinetic Monte Carlo model, Journal of Nuclear Materials 462 (2015) 91-99.
[31] M. Chiapetto, L. Malerba, C.S. Becquart, Effect of Cr content on the nanostructural evolution of irradiated ferritic/martensitic alloys: An object kinetic Monte Carlo model, Journal of Nuclear Materials 465 (2015) 326-336.
[32] L. Messina, M. Nastar, T. Garnier, C. Domain, P. Olsson, Exact ab initio transport coefficients in bcc Fe-X (X=Cr, Cu, Mn, Ni, P, Si) dilute alloys, Physical Review B 90(10) (2014).
[33] D. Stork, P. Agostini, J.L. Boutard, D. Buckthorpe, E. Diegele, S.L. Dudarev, C. English, G. Federici, M.R. Gilbert, S. Gonzalez, A. Ibarra, C. Linsmeier, A. Li Puma, G. Marbach, P.F. Morris, L.W. Packer, B. Raj, M. Rieth, M.Q. Tran, D.J. Ward, S.J. Zinkle, Developing structural, high-heat flux and plasma facing materials for a near-term DEMO fusion power plant: The EU assessment, Journal of Nuclear Materials 455(1-3) (2014) 277-291.
[34] B. Long, Y. Dai, N. Baluc, Investigation of liquid LBE embrittlement effects on irradiated ferritic/martensitic steels by slow-strain-rate tensile tests, Journal of Nuclear Materials 431(1-3) (2012) 85-90.

[35] M. Matijasevic, A. Almazouzi, Effect of Cr on the mechanical properties and microstructure of Fe-Cr model alloys after n-irradiation, Journal of Nuclear Materials 377 (2008) 147-154.
[36] M. Matijasevic, E. Lucon, A. Almazouzi, Behavior of ferritic/martensitic steels after n-irradiation at 200 and 300°C, Journal of Nuclear Materials 377 (2008) 101-108.
[37] N. Castin, G. Bonny, A. Bakaev, F. Bergner, C. Domain, J.M. Hyde, L. Messina, B. Radiguet, L. Malerba, The dominating mechanisms for the formation of solute-rich clusters in steels under irradiation, Acta Materialia submitted (2019) http://arxiv.org/abs/1912.06828.
[38] M.J. Konstantinovic, L. Malerba, Dissolution of carbon-vacancy complexes in Fe-C alloys, Phy Rev Mater 1(5) (2017).
[39] M.J. Konstantinovic, W. Van Renterghem, M. Matijasevic, B. Minov, M. Lambrecht, T. Toyama, M. Chiapetto, L. Malerba, Mechanical and microstructural properties of neutron irradiated Fe-Cr-C alloys, Phys Status Solidi A 213(11) (2016) 2988-2994.
[40] M.J. Konstantinovic, L. Malerba, Mechanical properties of FeCr alloys after neutron irradiation, Journal of Nuclear Materials 528 (2020) 151879.
[41] D. Terentyev, P. Olsson, L. Malerba, A. Barashev, Characterization of dislocation loops and chromium-rich precipitates in ferritic iron–chromium alloys as means of void swelling suppression
Journal of Nuclear Materials 362 (2007) 167-173.
[42] M. Hernandez-Mayoral, C. Heintze, E. Onorbe, Transmission electron microscopy investigation of the microstructure of Fe-Cr alloys induced by neutron and ion irradiation at 300 degrees C, Journal of Nuclear Materials 474 (2016) 88-98.
[43] L.L. Horton, J. Bentley, K. Farrell, A TEM STUDY OF NEUTRON-IRRADIATED IRON, Journal of Nuclear Materials 108(1-2) (1982) 222-233.
[44] V. Kuksenko, C. Pareige, P. Pareige, Cr precipitation in neutron irradiated industrial purity Fe-Cr model alloys, Journal of Nuclear Materials 432(1-3) (2013) 160-165.
[45] B. Gomez-Ferrer, C. Dethloff, E. Gaganidze, M.J. Konstantinovic, L. Malerba, B. Radiguet, A. Etienne, C. Pareige, APT measurements performed in the framework of the Nanohardening EP project, EUROfusion, CfP-AWP17-ENR-LPP-EMR-KLS-05 research project Final Report (2018).
[46] S.L. Dudarev, R. Bullough, P.M. Derlet, Effect of the alpha-gamma phase transition on the stability of dislocation loops in bcc iron, Physical Review Letters 100(13) (2008).
[47] J. Marian, B. Wirth, J. Perlado, Mechanism of formation and growth of <100> interstitial loops in ferritic materials, Physical Review Letters 88(25) (2002).
[48] H. Xu, R.E. Stoller, Y.N. Osetsky, D. Terentyev, Solving the Puzzle of <100> Interstitial Loop Formation in bcc Iron, Physical Review Letters 110 (2013) 265503.
[49] M.L. Jenkins, Z. Yao, M. Hernandez-Mayoral, M.A. Kirk, Dynamic observations of heavy-ion damage in Fe and Fe-Cr alloys, Journal of Nuclear Materials 389 (2009) 197-202.
[50] Z. Yao, M. Hernandez-Mayoral, M.L. Jenkins, M.A. Kirk, Heavy-ion irradiations of Fe and Fe-Cr model alloys Part 1: Damage evolution in thin-foils at lower doses, Philosophical Magazine 88(21) (2008) 2851-2880.
[51] M. Hernandez-Mayoral, Z. Yao, M.L. Jenkins, M.A. Kirk, Heavy-ion irradiations of Fe and Fe-Cr model alloys Part 2: Damage evolution in thin-foils at higher doses, philosophical Magazine 88(21) (2008) 2881-2897.
[52] D. Terentyev, L. Malerba, T. Klaver, P. Olsson, Formation of stable sessile interstitial complexes in reactions between glissile dislocation loops in bcc Fe, Journal of Nuclear Materials 382 (2008) 126-133.
[53] S.L. Dudarev, R. Bullough, P.M. Derlet, Effect of the alpha-gamma phase transition on the stability of dislocation loops in bcc iron, Physical Review Letters 100(13) (2008) 135503.
[54] D. Terentyev, T. Klaver, P. Olsson, M. Marinica, F. Willaime, C. Domain, L. Malerba, Self-trapped interstitial-type defects in iron, Physical Review Letters 100 (2008) 145503.

[55] T. D, I.M. Bragado, Evolution of dislocation loops in iron under irradiation: The impact of carbon, Scripta Materialia 97 (2015) 5-8.
[56] M. J. Konstantinović, A. Ulbricht, T. Brodziansky, N. Castin and L. Malerba, Vacancy-solute clustering in Fe-Cr alloys after neutron irradiation, J. Nucl. Mat. (2020) preprint.